Daytime longitudinal structures of electron density and temperature in the topside ionosphere observed by the Hinotori and DEMETER satellites

Y. Kakinami,[1,2] C. H. Lin,[3,4] J. Y. Liu,[1,5] M. Kamogawa,[6] S. Watanabe,[7] and M. Parrot[7]

[1]   Daytime longitudinal structures of the electron density (N_e) and temperature (T_e) in the topside ionosphere observed by Hinotori and DEMETER are examined under various conditions of solar flux, local time, and seasons. Results from both satellites show a similar longitudinal N_e structure in the morning from July to October, although the value of N_e observed by Hinotori is higher than that of DEMETER owing to higher solar flux. This result implies that the longitudinal structure of N_e may appear in any solar cycle. Further, a negative correlation between N_e and T_e in the longitudinal structures appears in the morning when N_e is low, while a positive correlation appears around the magnetic equator when N_e is sufficiently enhanced during noontime in the high solar flux. A spectrum analysis performed on the DEMETER data reveals that wave numbers 1–2 for N_e and T_e are dominant and nondominant. The observed wave numbers 3–4 for N_e are dominant during November–May and June–October, while they are dominant for T_e during October–June and July–September. Both N_e and T_e show the largest power of wave number 3 in December and wave number 4 in September. Further, observed annual variations of wave numbers 3–4 for N_e and T_e also differ from wave numbers 3–4 generated by waves in the lower thermosphere. It can be interpreted as discrepancies between the longitudinal distributions of N_e and T_e caused by difference in the condition of zonal winds driving E region dynamo and meridional winds modulating the ionospheric plasma structures.

Citation: Kakinami, Y., C. H. Lin, J. Y. Liu, M. Kamogawa, S. Watanabe, and M. Parrot (2011), Daytime longitudinal structures of electron density and temperature in the topside ionosphere observed by the Hinotori and DEMETER satellites, *J. Geophys. Res.*, *116*, A05316, doi:10.1029/2010JA015632.

1. Introduction

[2]   Electron density (N_e) in the ionosphere is produced by solar EUV radiation, since the solar photons have significant energy to ionize the neutral atmosphere. Simultaneously, photoelectrons produced in this ionization process heat the local ambient electrons as well as remote electrons along the magnetic field line. Electron temperature (T_e) is governed by heating of photoelectron, cooling caused by collisions among ions and neutral species, and heat conduction in the ionosphere [e.g., *Watanabe et al.*, 1995]. Below 200 km, the collision cooling of electron with the neutral atmosphere is dominant because of the high neutral density [*Bilitza*, 1987]. Above 200 km, N_e controls T_e, and T_e shows a negative correlation with N_e, because the Coulomb collision cooling, of which rate is proportional to the square of N_e [*Schunk and Nagy*, 1978], dominates the heat balance of electrons [*Bilitza*, 1975; *Brace and Theis*, 1978]. In the topside ionosphere (above the F_2 peak), the heat conduction becomes a dominant factor because the number of the collisions decreases. Therefore T_e is not controlled by the local variation of N_e but rather by integrated N_e along the corresponding magnetic field line below the F_2 peak.

[3]   Large-scale electric fields are generated by the interaction between the neutral atmosphere and the plasma around 100 km. The plasma is transported upward by the $\mathbf{E} \times \mathbf{B}$ drift around the magnetic equator, where $\mathbf{E}$ and $\mathbf{B}$ are the electric and the magnetic field, so that the plasma forms the equatorial ionization anomaly (EIA) when diffusing poleward along the magnetic field line [e.g., *Namba and Maeda*, 1939; *Appleton*, 1946], which is named fountain effect. In particular, the large-scale electric field at the magnetic equator also

[1]Institute of Space Science, National Central University, Jhongli, Taiwan.

[2]Now at Institute of Seismology and Volcanology, Hokkaido University, Sapporo, Japan.

[3]Department of Earth Science, National Cheng Kung University, Tainan, Taiwan.

[4]Also at Earth Dynamic System Research Center, National Cheng Kung University, Tainan, Taiwan.

[5]Also at Center for Space and Remote Sensing Research, National Central University, Jhongli, Taiwan.

[6]Department of Physics, Tokyo Gakugei University, Tokyo, Japan.

[7]Department of Cosmoscience, Hokkaido University, Sapporo, Japan.

drives the equatorial electrojet (EEJ) [*Forbes*, 1981; *Fang et al.*, 2008, and references therein], which is detected on the ground as variations of the magnetic field. Thermospheric winds also transport the plasma in the topside ionosphere upward/downward along the magnetic field line [*Watanabe and Oyama*, 1996].

[4] Recently, several studies of coupling between the ionosphere and the thermosphere as well as between the ionosphere and the troposphere have been reported. An eastward propagating diurnal tide with zonal wave number 3 (DE3) excited by tropical tropospheric latent heat release modulates the lower thermospheric winds [*Hagan et al.*, 2007], resulting in modulation of the electric field in the lower ionosphere [*Immel et al.*, 2006]. The modulated electric field produces wave number 4 longitudinal structure in the EIA region. The wave number 4 longitudinal structure was first found by the observation of OI 135.6 nm emission during nighttime [*Sagawa et al.*, 2005; *Immel et al.*, 2006]. Similar wave number 4 longitudinal structures have been reported in electron density profiles obtained by occultation technique [*Lin et al.*, 2007a], total electron content (TEC) [*Lin et al.*, 2007b; *Scherliess et al.*, 2008; *Wan et al.*, 2008], ion density [*Liu and Watanabe*, 2008; *Pedatella et al.*, 2008], vertical $\mathbf{E} \times \mathbf{B}$ drift velocity [*Kil et al.*, 2007], EEJ [*England et al.*, 2006], and thermospheric zonal winds [*Häusler and Lühr*, 2009]. *Jin et al.* [2008] numerically demonstrated that DE3 propagates to the *E* region dynamo layer and perturbs the electric field owing to a Hall dynamo current. The longitudinal structure appears before 0900 LT (local time) and is amplified during the afternoon [*Lin et al.*, 2007b; *Kil et al.*, 2008]. The structure decays during the night [*Lin et al.*, 2007b; *England et al.*, 2008; *Bankov et al.*, 2009].

[5] The longitudinal structure shows an annual variation. The wave number 4 longitudinal structure of TEC appears around the equinox and June solstice but disappears around the December solstice [*Scherliess et al.*, 2008]. The wave number 4 longitudinal structure of N_e at 400 km was observed by the CHAMP satellite for September equinox [*Liu and Watanabe*, 2008], and by FORMOSAT-3/COSMIC during September–October [*Lin et al.*, 2007a]. *Kil et al.* [2008] also show that the wave number 4 longitudinal structure of N_e above 600 km appears around equinoxes and June solstice. Furthermore, a wave number 3 longitudinal structure of N_e possibly appears during other months [e.g., *Scherliess et al.*, 2008; *Lin et al.*, 2011]. *Ren et al.* [2008] reported on longitudinal variations of ion density (N_i) and T_e at 800 km by using 11 year DMSP satellite data. They analyzed 4 month averaged data of the total 11 year period regardless of solar activities and showed that wave number 4, 3, and 2 longitudinal structures appear during equinoxes, May–August, and November–February, respectively. According to their results, the observed wave numbers are highly expected to depend on seasons. Further, *Häusler and Lühr* [2009] showed annual variations of several oscillations in the thermospheric zonal winds and reported a maximum amplitude of the wave number 4 longitudinal structure during July–October and a second maximum amplitude during March–April. The authors attributed the observed wave numbers 3–4 structure to the influence of eastward propagating diurnal tide with zonal wave number 2 (DE2) and DE3. *Pedatella et al.* [2008] also reported annual variations of DE2 and DE3 at 100 km, of which the amplitudes dominate during December–February

and March–September. In addition, diurnal neutral temperature amplitude revealed that the wave number 4 structure appears during July–September around 100 km in the ionospheric dynamo region [*Forbes et al.*, 2008]. Annual variations of the wave number 3–4 longitudinal structures in the topside ionosphere are therefore expected to play a major role in understanding coupling mechanisms between the thermosphere and the ionosphere.

[6] In this paper, we thus use daytime measurements by the Hinotori and DEMETER satellites to investigate the longitudinal structure of N_e and T_e in different solar fluxes. While the Hinotori satellite performed its measurements in high solar flux, the solar flux was low during DEMETER measurements. A spectrum analysis of monthly data is conducted to compare with the tidal signature in the neutral atmosphere reported by *Pedatella et al.* [2008] and *Häusler and Lühr* [2009]. Finally, discrepancies between tidal signatures of N_e and T_e are discussed.

2. N_e and T_e Obtained by the Hinotori Satellite

[7] The Hinotori satellite, which was a solar observation satellite, housed an impedance probe for N_e measurement [*Oya et al.*, 1986] and a temperature probe for T_e measurement [*Hirao and Oyama*, 1970; *Oyama et al.*, 1988]. The Hinotori satellite has revealed N_e and T_e variations of seasons [*Su et al.*, 1998; *Bailey et al.*, 2000], local time (LT) [*Watanabe et al.*, 1995; *Oyama et al.*, 1996], and magnetic disturbances during high solar activity [*Oyama et al.*, 2005] at 600 km altitude. The measurements of T_e and N_e by the Hinotori satellite were operated for 16 months, from February 1981 to June 1982. The satellite was put into a circular orbit, non-Sun-synchronous orbit with an inclination of 31°. The satellite measured a region within ±32° latitude for any LT and longitude except the southern Pacific Ocean and northern Antarctica owing to the limitation of the onboard data storage [see *Kakinami et al.*, 2008]. Further, T_e and N_e data were not stored during solar flares because data recording of the other instruments was prioritized [*Watanabe and Oyama*, 1996]. The orbital period was about 90 min, and approximately 2 months were required to return to the same orbit.

[8] The data measured by the Hinotori satellite from July to October 1981 are analyzed under the magnetic condition of $Kp < 4$. Minimum, maximum, and average values of the solar flux index $F_{10.7}$ (in 10^{-22} W/m^2 Hz) are equal to 143, 305, and 214 during this period, respectively. Medians of N_e and T_e are calculated for bins sized with 30° longitude and 15° latitude with shifting in the steps of 10° longitude and 5° latitude. The bins containing less than 30 data points are dismissed from the analysis. Figure 1 illustrates the spatial distributions of the N_e and T_e medians during 0900–1100 LT. High N_e is observed near the magnetic equator and N_e decreases with increasing latitudes (Figure 1a). Errors, defined by the difference between first and third quartiles, for N_e along the magnetic equator are within −70–270% of the median values around 5, 115 and 305°E and −50–50% except the regions of 5, 115 and 305°E. Note that 69 percentile of N_e at the largest 270% error (i.e., at 305°E) is lower than 31 percentile at the neighboring maximum of median at 275°E. The errors for T_e are within −20–25% of median values at the magnetic equator of all longitudes. Three maxima of N_e are clearly identified around 95°, 185°,
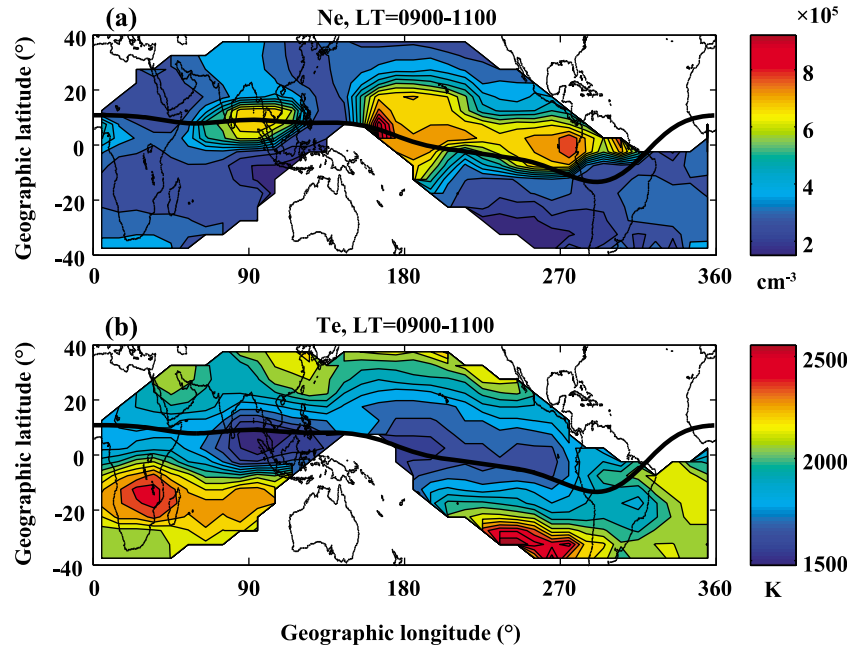
Figure 1. (a) N_e and (b) T_e distributions measured by the Hinotori satellite during 0900–1100 LT from July to October 1981. Medians of N_e and T_e are calculated for 30° longitude and 15° latitude sized bins which are shifted in steps of 10° longitude and 5° latitude. Black curves indicate the magnetic equator.

and 275°E in the vicinity of the magnetic equator. Since data are out of record around 330°E in the Northern Hemisphere, the existence of a fourth maximum is not confirmed. However, a weak N_e enhancement is detected around 0°E. The highest N_e maximum with a value of 9.7×10^5 cm^{-3} is located at 165°E. The N_e maximum at 185°E expands widely from 25°N to 20°S. The distribution of T_e corresponds to the inverse one of N_e (Figure 1b). Since T_e shows a negative correlation with N_e, lower T_e is observed around the magnetic equator and T_e increases with increasing latitudes. Three T_e minima are identified at 95°, 175°, and 265°E along the magnetic equator. The locations of T_e minima almost coincide perfectly with the longitudes of N_e maxima. Though a clear minimum of T_e is not identified around 330°E owing to lack of data, low T_e is observed around 0°E at the magnetic equator. The T_e minimum around 175°E has the widest latitudinal range from 20°N to 15°S, and it corresponds to the N_e maximum at the same longitude.

[9] Figure 2 illustrates the N_e and T_e distributions during 1300–1500 LT. The errors for N_e and T_e are within −20–20% and −20–10% of the median values around the magnetic equator, respectively. There is an enhancement of N_e around the magnetic equator with an expansion to higher latitudes up to about ±20° magnetic latitude, owing to the plasma fountain effect, and a decrease with increasing latitudes outside the EIA region (Figure 2a). The major N_e maxima are observed at 15°, 135°, 215°, and 285°E. Comparing Figures 1a and 2a, the maxima of N_e shift eastward, while other two small maxima of N_e located at conjugate points appear around 90°E, showing a typical EIA feature. In Figure 2b (1300–1500 LT), T_e shows a positive correlation with N_e, and the highest T_e maximum locates at 235°E. Another small T_e maximum is seen at 275°E. Except for these two longitude

areas, it is difficult to detect T_e maximum on other longitudes. It is noted that T_e shows again a negative correlation with N_e outside the EIA region.

[10] Figure 3 displays N_e and T_e distributions for 1300–1500 LT in the months of April–July in 1981 and 1982 under geomagnetically quiet condition of $Kp < 4$. Minimum, maximum, and average values of $F_{10.7}$ are equal to 94, 287, and 176 during this period, respectively. The errors for N_e are within −40–90% of the median values around the magnetic equator. The errors for T_e are within −6–35% of the median values around the magnetic equator. There are three major maxima of N_e comprising several small peaks around the magnetic equator at 0°, 105°, and 215°E. The largest value of N_e maximum around 105°E is 1.3×10^6 cm^{-3}. The N_e of April–July (Figure 3a) is globally lower than that of July–October (Figure 2a). In Figure 3b, T_e increases with increasing latitude. In contrast to Figure 2b, a maximum of T_e in April–July does not clearly appear around the magnetic equator. Clear longitudinal wave structure of T_e is not detected, and the only T_e minimum is at 179–285°E with a value of 1452 K. The location of the T_e minimum does not correspond to the N_e maxima.

3. N_e and T_e Obtained by the DEMETER Satellite

[11] The French microsatellite DEMETER (Detection of Electro-Magnetic Emissions Transmitted from Earthquake Regions) was launched on 29 June 2004 and put into a circular and quasi-Sun-synchronous orbit with an inclination of 98°. Descending and ascending nodes are at 1030 and 2230 LT. Altitude of DEMETER was 710, 680, and 660 km from June 2004 to December 2005, to January 2006, and to December 2010, respectively. The orbital period is about
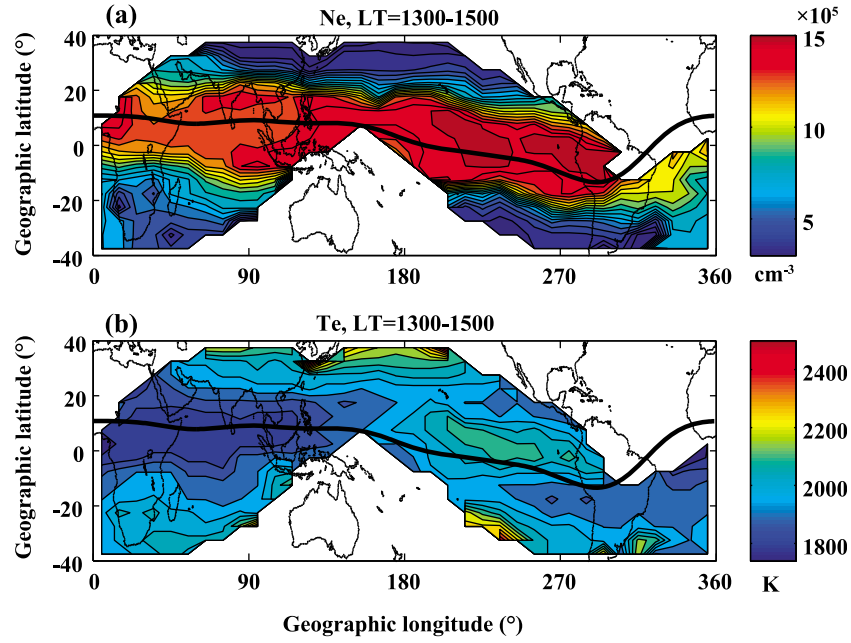
Figure 2. The same as Figure 1 but for 1300–1500 LT.

100 min, and all longitudes are covered within ±65° geomagnetic latitude. The DEMETER satellite houses a Langmuir probe named Instrument Sonde de Langmuir (ISL), which measures N_e in the range of 10^2–5×10^5 cm^{-3} and T_e in the range of 600–10,000 K [*Lebreton et al.*, 2006].

[12] For comparison with the results obtained by the Hinotori satellite, the data are accumulated under the magnetic condition of $Kp < 4$ from July to October 2007. During this period, the minimum, maximum, and average values of the solar activity $F_{10.7}$ are equal to 65, 79, and 68, respectively. Medians of N_e and T_e are calculated for bins sized

with 15° longitude and 9° latitude with shifting in the steps of 5° longitude and 3° latitude between ±60° geomagnetic latitude. The spatial distributions of the medians of N_e and T_e for 1030 LT are shown in Figures 4a and 4b, respectively. Errors for N_e and T_e are within −30–50% and −20–5% of the median values around the magnetic equator, respectively. High values of N_e are found at the magnetic equator, and they decrease with increasing latitudes. The longitudinal variations of N_e measured by the DEMETER satellite are similar to those measured by the Hinotori satellite. Four maxima of N_e are located at 98°, 193°, 253°, and 353°E with magnitude
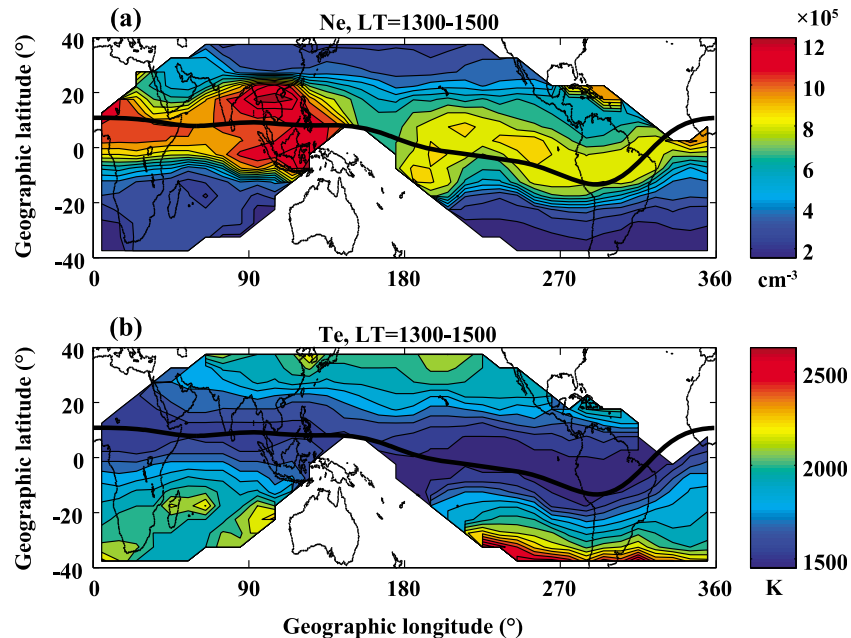

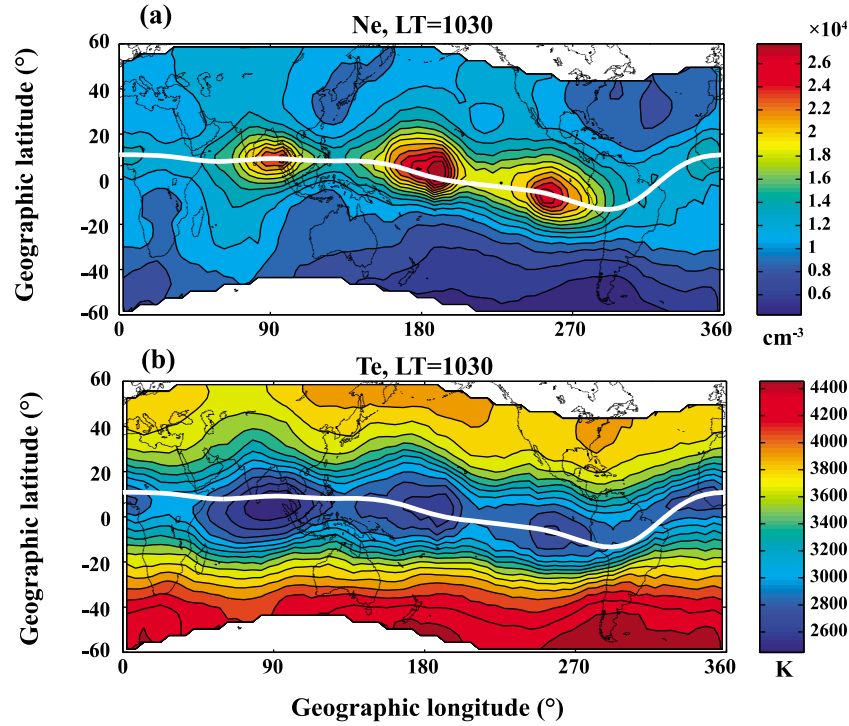**Figure 3.** The same as Figure 2 but for April–July in 1981 and 1982.

Figure 4. (a) N_e and (b) T_e distributions measured by the DEMETER satellite at 1030 LT from July to October 2007. Medians of N_e and T_e are calculated for 15° longitude and 9° latitude sized bins which are shifted in steps of 5° longitude and 3° latitude between ±60° geomagnetic latitude. White curves indicate indicates the magnetic equator.

of 2.5×10^4, 2.9×10^4, 2.7×10^4, and 1.5×10^4 cm^{-3}, respectively. The highest and lowest values of N_e maxima are seen at 193° and 353°E, respectively. The highest N_e maximum corresponds to the widest latitude range (30°N–20°S), which indicates that the plasma is transported by a strong $\mathbf{E} \times \mathbf{B}$ drift at the magnetic equator and diffuses along the magnetic field line toward high latitudes. Meanwhile, values of T_e are lower around the magnetic equator and increase with increasing latitudes. Minima of T_e around the magnetic equator are located at 88°, 193°, 258°, and 353°E. Locations of local N_e maximum and T_e minimum are very close to each other. However, the lowest value of T_e minimum is not observed at the location of the highest value of N_e maximum.

4. Annual Variation of N_e and T_e Observed by the DEMETER Satellite

[13] To investigate the annual variation of N_e and T_e, DEMETER data are accumulated under geomagnetically quiet conditions ($Kp < 3$) from 2006 to 2007. During this period, minimum, maximum, and average $F_{10.7}$ are equal to 65, 103, and 77, respectively. Sixty-day running medians for N_e (Figure 5) and T_e (Figure 6) at 1030 LT are calculated for bins sized with 15° longitude and 9° latitude with shifting in the steps of 5° longitude and 3° latitude between ±60° geomagnetic latitude, respectively. Errors for N_e and T_e are within −45–80% and −15–15% of the median values around the magnetic equator throughout the year. As shown in Figures 1–4, N_e also shows maxima around the magnetic equator and decreases toward higher latitudes in all months.

Clear EIA structures are not observed because the fountain effect does not sufficiently reach the satellite altitude (660 km) under solar minimum conditions owing to reduced intensity of $\mathbf{E} \times \mathbf{B}$ drift [Fejer, 1991; Liu et al., 2007]. Owing to neutral wind effects, the maxima of N_e are shifted northward around the June solstice in the regions of positive declination (180–285°E), and shifted southward around December solstice in the region of negative declinations (285–360°E) [Watanabe and Oyama, 1996; Oyama et al., 1996]. In addition, a clear longitudinal structure of N_e is detected around the magnetic equator in all months, but the number of N_e maxima varies throughout the year. The highest value of N_e maximum often appears around 190°E. Meanwhile, the maximum of N_e around 330°E is very low from May to August. The global N_e intensity shows large values around March and October while it shows small values in June and July. A semiannual variation of N_e is shown around 190°E at the magnetic equator amounting to 4.8×10^4, 2.1×10^4, 5.2×10^4, and 3.2×10^4 cm^{-3} in March, July, October, and December, respectively. This semiannual variation of N_e mainly comes from the ratio of O to N_2 [e.g., Su et al., 1998] because an increase of O and N_2 gives rise to an increase of the production and recombination rate of the plasma, respectively.

[14] Figure 6 shows that T_e minima appear at N_e maximum structure appearing as T_e minima along the magnetic equator, and T_e increases with increasing latitudes. A longitudinal structure of T_e around the magnetic equator is also similar to that of N_e. In general, since N_e correlates with T_e above 200 km during the daytime owing to the cooling rate of electron proportional to the square of N_e [Bilitza, 1975; Brace
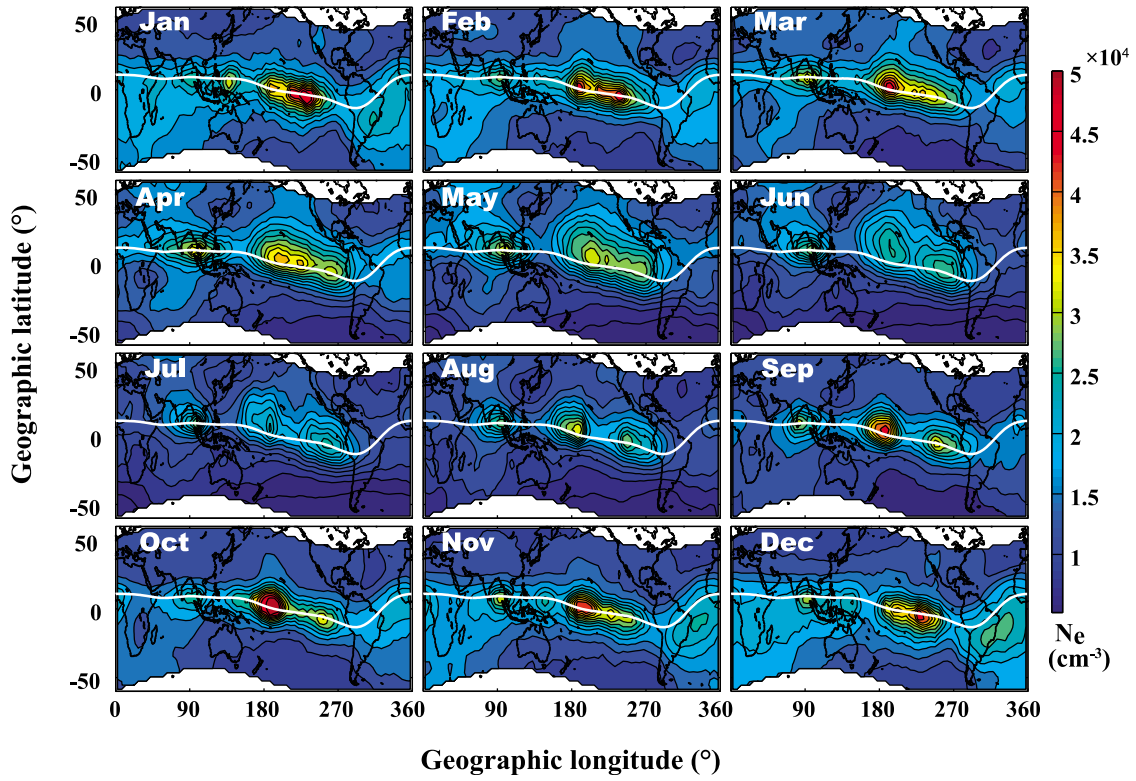
Figure 5. Annual variation of N_e measured by the DEMETER satellite at 1030 LT during 2006–2007. Sixty-day running medians for N_e are calculated for 15° longitude and 9° latitude sized bins which are shifted in steps of 5° longitude and 3° latitude between ±60° geomagnetic latitude. White curves indicate the magnetic equator.

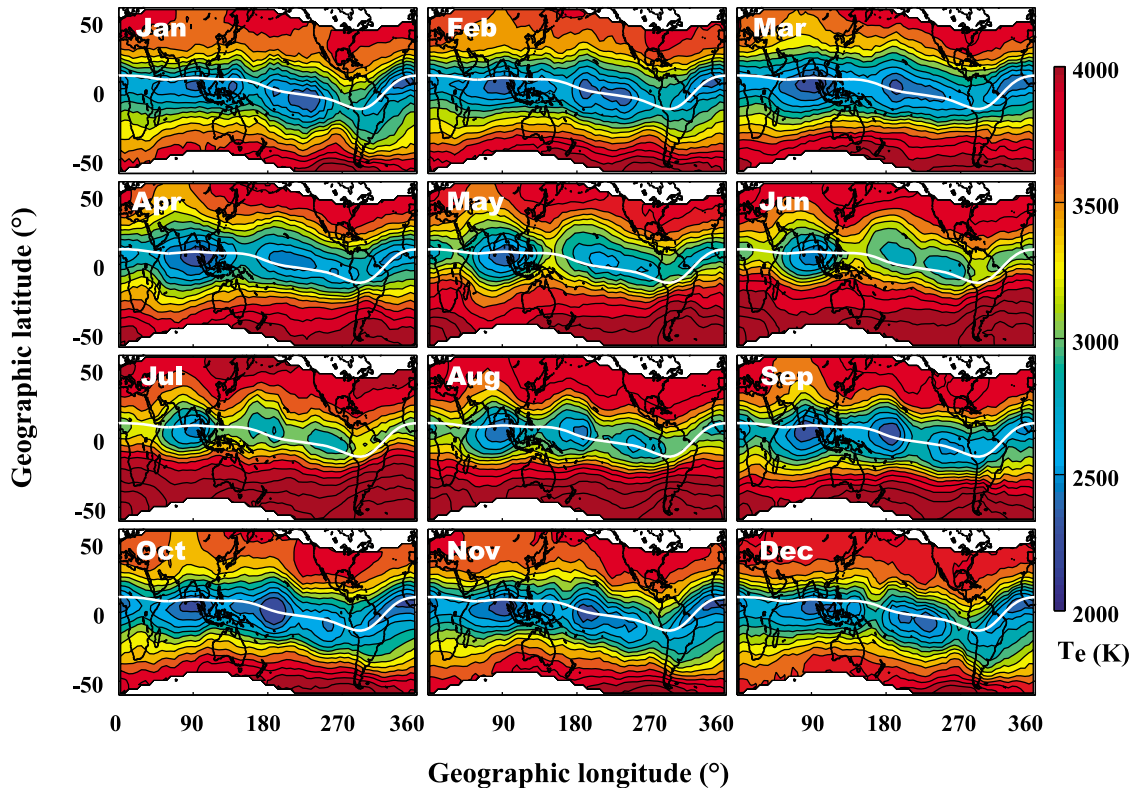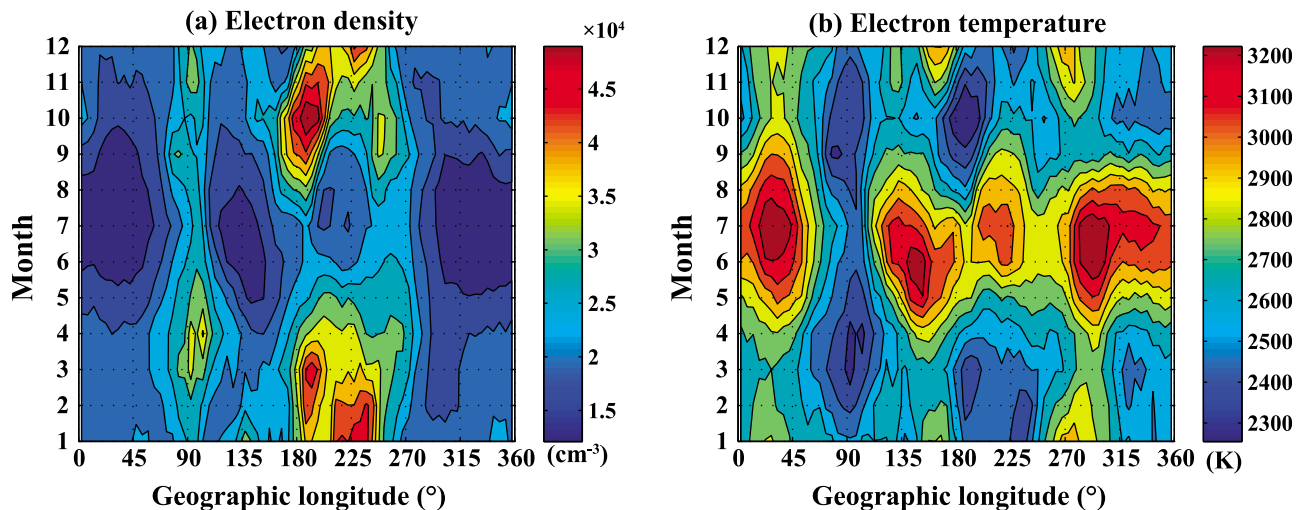**Figure 6.** The same as Figure 5 but for T_e.

Figure 7. Annual variation of 60 day running median of (a) N_e and (b) T_e within ±5° magnetic dip latitude. Medians of N_e and T_e are calculated for 15° longitude sized bins which are shifted in steps of 5° longitude.

and Theis, 1978; *Bilitza and Hoegy*, 1990], enhanced N_e is typically accompanied by a reduction of T_e. However, the most pronounced minimum of T_e often appears around 90°E, while the N_e maximum around 90°E is not always the most distinct one. Further, N_e maxima at 330°E are very weak, while the T_e minimum always exists around 330°E. Although spatial distributions of T_e and N_e are clearly inversely correlated, their intensities in the minima and maxima are not always inversely correlated. This suggests that T_e does not completely correlate with the in situ observed N_e.

[15] To investigate the annual variation at the magnetic equator, 60 day running medians of N_e (Figure 7a) and T_e (Figure 7b) within ±5° magnetic dip latitude are calculated for bins sized with 15° longitude with shifting in the steps of 5° longitude. Maxima of N_e are located around 90° and

190°E during the whole year while the maximum at 230°E is shifted to 250°E during April–October. As illustrated in Figure 5, the maximum of N_e around 190°E becomes the highest during August–March. The maximum of N_e around 330°E is always the lowest during September–April and almost disappears during May–August. As shown in Figure 7b, the minima of T_e are almost located around 90°, 190°, 250°, and 330°E. Although the maximum of N_e at 190°E is larger than the other maxima of N_e during August–March, the minimum of T_e at 190°E is not always the lowest minimum. The most pronounced minimum of T_e occurs at 90°E during February–September. When the T_e minimum at 250°E is close to the minimum at 190°E, a wave number 3 longitudinal structure becomes dominant. This feature is the same as one of the distribution of N_e.
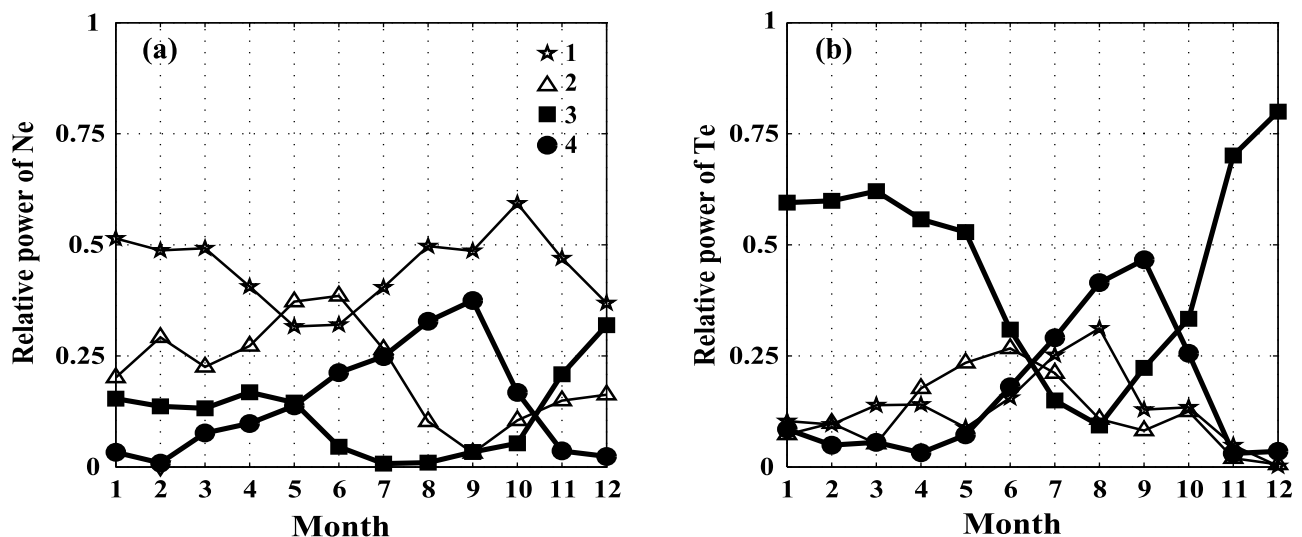

Figure 8. Annual variation of normalized wave power of (a) N_e and (b) T_e at the magnetic equator. A spectrum analysis is applied to the data shown in Figure 7. The star, triangle, square, and circle denote wave numbers 1, 2, 3, and 4, respectively.

[16] A spectrum analysis is applied to the longitudinal median values of N_e and T_e shown in Figure 7. Thereby, each wave number power is normalized by the integrated power of all wave numbers, and the results are displayed in Figure 8. Since power of wave number 5 and larger are very weak (less than 0.01), only results for wave numbers 1–4 are shown. For wave numbers 3–4, the spectrum of both the N_e and T_e show that the power is the largest in December and September, respectively. For wave numbers 1–2, the spectrum of N_e shows that the powers are significant while the spectrum of T_e shows that the powers are weak in the whole months. In addition, the spectrum shows that wave number 3 in N_e and T_e is larger and smaller than wave number 4 in June, respectively. The spectrum analysis verifies the discrepancies of the seasonal variation of longitudinal N_e and T_e structures.

5. Discussion

[17] From the results of the Hinotori and DEMETER satellites, pronounced maxima of N_e around 1030 LT are similarly located in Southeast Asia (90°E), the Pacific Ocean (190°E), and west of South America (230°–250°E) in the different solar fluxes. Note that the maximum located in the Atlantic Ocean (330°E) was only detected by the DEMETER satellite and not detected by the Hinotori satellite owing to the restricted observation coverage. The N_e measured by the Hinotori satellite is generally higher than that by the DEMETER satellite owing to the higher solar flux. Minima of T_e observed by both satellites also appear at similar locations and the lowest minimum of T_e appears in Southeast Asia (90°E). The results obtained by the Hinotori satellite show that the N_e maxima propagate eastward when LT advances, following those by the FORMOSAT3/COSMIC satellites [*Lin et al.*, 2007b]. However, the present spatial (10° longitude) and temporal (60 days in 2 h LT) resolution, which is needed at least to indentify the longitudinal structures from Hinotori data, is not sufficient to estimate accurate propagation velocity.

[18] Negative correlation between N_e and T_e as shown in Figures 1 and 4 is obtained in the morning of both low and high solar flux levels. It is also obtained even around noontime in high solar flux when N_e is low (Figure 3). This negative correlation is caused by the cooling process of electrons, of which the rate is proportional to square of N_e [*Bilitza*, 1975; *Brace and Theis*, 1978; *Bilitza and Hoegy*, 1990]. However, the positive correlation between N_e and T_e around the magnetic equator is seen during noontime when N_e is sufficiently enhanced (Figure 2).

[19] When N_e is high, cooling due to the Coulomb collision becomes more effective for electrons below the F_2 peak, so that the electron and ion temperature (T_i) become closer to neutral temperature (T_n). In other words, T_e and T_n vary together for high N_e. *Lei et al.* [2007] numerically demonstrated that the positive correlation between N_e and T_e at the F_2 peak support observations made by incoherent scatter radars at Millstone Hill and Arecibo. In their interpretation, the positive correlation means that T_e increases with T_n because both N_e and T_n increase with solar activity. It implies that besides the solar flux variation, the positive correlation may also occur under condition of simultaneous increase of N_e and T_n. We emphasize that the longitudinal

structure of N_e is not caused by the solar flux variation. According to *Liu et al.* [2009], N_e and neutral density (N_n) are roughly inversely correlated in the longitudinal structure; that is, low N_n is observed for high N_e. Since high N_n region generally shows high T_n under hydrostatic equilibrium, T_n is highly expected to be low at the high N_e, i.e., a negative correlation between N_e and T_n. Therefore, in order to explain the positive correlation between N_e and T_e, other interpretations are required. We need future investigation to solve this issue.

[20] The most pronounced N_e maximum around 190°E is seen during August–March, whereas the N_e maximum observed around 330°E is the weakest (Figure 7a). *Kil et al.* [2007] showed a similar distribution of N_e measured by the ROCSAT-1 satellite. However, $\mathbf{E} \times \mathbf{B}$ drift measured by the ROCSAT-1 satellite, which might be the primary driver to modulate intensity of the plasma fountain effect as well as the N_e in the topside ionosphere, does not show the similar locations of maximum (~190°E) and minimum (~330°E) as shown by Hinotori and DEMETER. These results imply that N_e in the topside ionosphere may not be affected only by $\mathbf{E} \times \mathbf{B}$ drift. The N_e maximum is located around 230°E during December–March, while it is relocated around 250°E during April–October. *Forbes et al.* [2009] reported that the temperature maximum located around 270°E moves to 240°E from September 2005 to January 2006 at 110 km altitude. Their result implies that the driver producing longitudinal structure in the topside ionosphere possibly moves. The similar westward movement of N_e maximum in the topside ionosphere suggests that our results are highly connected to the movement of the driver in the mesosphere and lower thermosphere (MLT) region.

[21] Annual variation of the longitudinal structures at different altitudes has been discussed in several relevant studies. DE3, corresponding to wave number 4 longitudinal structure observed by satellites slowly precessing in LT, is dominant during July–September at 95 km [*Forbes et al.*, 2003]. Diurnal neutral temperature amplitude revealed that the wave number 4 longitudinal structure appears during July–September around 100 km in the ionospheric dynamo region [*Forbes et al.*, 2008]. The wave number 4 longitudinal structure of zonal wind measured by the SABER and TIDI, on board the TIMED satellite, is dominant at 100 km in August [e.g., *Pedatella et al.*, 2008]. The strongest wave number 4 signature in the zonal wind around 400 km appears during July–October [*Häusler and Lühr*, 2009]. Moreover, the neutral density at 400 km measured by the CHAMP satellite also shows the wave number 4 longitudinal structure around equinoxes [*Liu et al.*, 2009]. The CHAMP satellite shows that the wave number 4 of N_e appears around 350–420 km in July [*Pedatella et al.*, 2008]. *Kil et al.* [2008] pointed out that the wave number 4 longitudinal structure of N_e appears at 600 km and above around equinoxes and June solstice. Similarly, *Ren et al.* [2008] showed the wave number 4 longitudinal structure of N_e and T_e at 600 and 850 km around equinoxes. The results of both neutral atmosphere and N_e suggest that the wave number 4 longitudinal structure dominates during July–September. Besides wave numbers 1 and 2, the wave number 4 longitudinal structure of N_e measured by the DEMETER satellite is significantly seen during June–October, while the wave number 4 longitudinal structure of T_e measured by the DEMETER satellite is the strongest wave
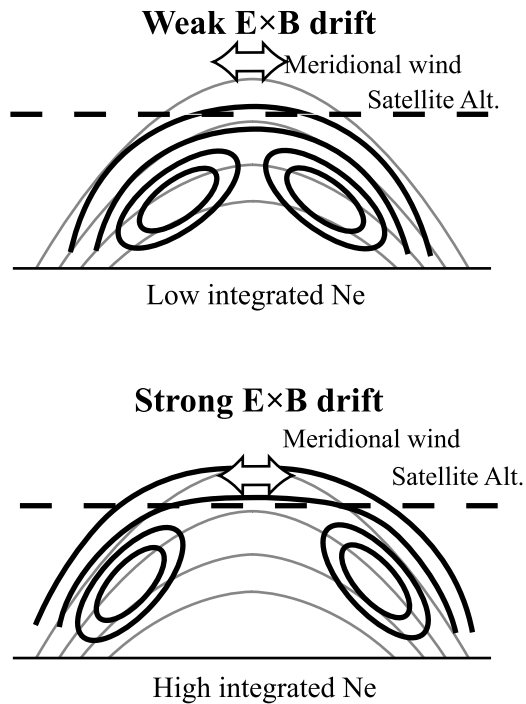
Weak E×B drift

Strong E×B drift

Figure 9. Sketch showing the fountain effect and the meridional neutral winds which affect N_e and T_e in the top-side ionosphere. Black curves, gray curves, and horizontal dash lines denote contour of N_e, the magnetic field lines, and the satellite altitudes, respectively. Arrows indicate the meridional winds. This sketch demonstrates that the in situ N_e measurement at the satellite altitude may not reflect the strength of the plasma fountain as clear as integrated N_e along the magnetic field lines. Therefore, the T_e, which is highly correlated with the integrated N_e, and N_e shown in this study do not correlate perfectly with each other.

number during July–September. The most pronounced amplitudes of wave number 4 of N_e and T_e are detected in September. All measurements introduced in this paragraph support our observation result that the wave number 4 is the most pronounced in September.

[22] In addition, DE2 producing the wave number 3 longitudinal structure in the neutral temperature becomes dominant during November–June [*Forbes et al.*, 2008]. However, *Pedatella et al.* [2008] reported that amplitudes of zonal wind of DE2 and SW4 (westward propagating semidiurnal tide with zonal wave number 4) at 100 km only exceed those of DE3 and DE2 during December–February and January–February, respectively. *Oberheide and Forbes* [2008] also reported similar results in neutral density at 100 km altitude. *Kil et al.* [2008] reported that either wave number 3 or 4 longitudinal structure of N_e appears around December solstice because the maxima at 150°–300°E have one or two peaks. These results differ from the intensity of wave numbers 3 and 4 longitudinal structures of N_e and T_e obtained by the DEMETER satellite, where the intensity of the wave number 3 longitudinal structure exceeds that of the wave number 4 during November–April for N_e and October–June for T_e (Figure 8). The annual variation of the wave number 3 of our result does not exactly correspond to the observed annual variation of DE2 in the MLT. Therefore, our results

suggest that the N_e and T_e at the topside ionosphere may not be solely affected by the nonmigrating tides around the dynamo region but also by other drivers, such as meridional neutral winds in the topside ionosphere which push up and down plasma along the magnetic field.

[23] Longitudinal structures of N_e and T_e obtained by the DEMETER satellite are not completely consistent with each other. Although the N_e maxima and the T_e minima roughly occur at the same locations, the locations of the highest N_e maximum value and the lowest T_e minimum value do not always occur exactly at the same locations. The lowest T_e minimum value and the highest N_e maximum value are observed around 90°E during February–September and around 190°E during August–March, respectively. These results indicate that in situ T_e is not completely correlated with in situ N_e in the topside ionosphere. Spectrum analyses also show the different behaviors between N_e and T_e. While wave numbers 1–2 in N_e are roughly dominant in all months, the amplitudes of wave numbers 1–2 in T_e are lower than those of wave number 3 or 4. Zonal wind influenced by nonmigrating tides modulates zonal electric field [e.g., *Jin et al.*, 2008]. The modulated **E** × **B** drift produces longitudinal structure of N_e in the topside ionosphere. If the equatorial plasma fountain effect is not strong enough to transport the plasma to topside ionosphere, N_e enhancement is not detected there because the plasma is not supplied to the topside ionosphere. Therefore, even if wave numbers 3 and/or 4 of zonal winds dominate in the ionosphere/thermosphere lower than the satellite altitude, they are not detected in the topside ionosphere. As a result, one or two peaks is only detected clearly, and then the wave numbers 1 and/or 2 become dominant only for N_e.

[24] In general, the T_e in the ionosphere is governed by the heat balance between photoelectron heating, Coulomb collision cooling, and heat conduction along the magnetic field line. In the topside ionosphere where the heat conduction is dominant, T_e is not governed by in situ N_e but by N_e integrated along the magnetic field line below the F_2 peak. In Figure 9 (bottom), the in situ N_e at the satellite altitude around equator trough may not show large magnitude during strong plasma fountain. The strong fountain effect may transport N_e at the equator into neighboring high latitudes, resulting in a decrease of the plasma at the magnetic equator trough. However, the integrated N_e along the field line below the F_2 peak would reveal stronger magnitude during the strong plasma fountain than during the weak plasma fountain as illustrated in Figure 9 (top), since the EIA peaks of strong fountain shift to high latitudes where their associated magnetic field lines reach the satellite altitude. As a result, the in situ N_e measurement at the satellite altitude does not completely correlate with the integrated N_e. Additionally, the meridional wind can transport the plasma and affect the N_e magnitude around the magnetic equator [e.g., *Lin et al.*, 2005]. Therefore, the in situ N_e distribution measured by the DEMETER satellite may not represent the stronger or the weaker EIA as clearly as the T_e distribution, since T_e is highly relevant to the N_e integrated along the magnetic field line.

6. Conclusion

[25] This study examines daytime topside-ionospheric longitudinal structures of N_e and T_e measured by the Hinotori

and DEMETER satellites. Both satellite measurements show similar longitudinal structures of N_e and T_e in the morning even in different solar fluxes. This fact suggests that these longitudinal structures appear in any solar flux. In the morning, T_e shows a negative correlation with N_e at any latitude and in any solar flux when N_e is low. However, during noontime for high solar flux, T_e shows a positive correlation with N_e around the magnetic equator when N_e is sufficiently enhanced. Although the wave numbers 1 and 2 in N_e dominate the other wave numbers, those wave numbers in T_e are very weak. Besides the wave numbers 1 and 2, the wave numbers 3 and 4 of N_e are dominant during November–April and June–October, respectively. Meanwhile, the wave numbers 3 and 4 of T_e are dominant during October–June and July–September, respectively. These results reveal that annual variation of N_e and T_e in the topside ionosphere does not fully correspond with annual variation of DE2 and DE3 in the dynamo region as reported by *Pedatella et al.* [2008] and at 400 km reported by *Häusler and Lühr* [2009]. Meanwhile, locations of the longitudinal structures of N_e and T_e do not perfectly match each other. These results may be caused not only by zonal wind driven by dynamo effects but also by meridional winds which may modify the longitudinal structures of N_e in the topside ionosphere. Therefore, our results suggest that the longitudinal structure of N_e in the topside ionosphere is produced not only by the modulated electric field by nonmigrating tides in the dynamo region but also by meridional wind effects at the satellite altitude. As T_e is mainly affected by the integrated N_e below the F_2 peak, the modification of the T_e by the meridional wind effect is not as prominent as in the N_e. Therefore, T_e is a better indicator for nonmigrating tidal effect at topside ionosphere than the N_e.

References

Appleton, E. V. (1946), Two anomalies in the ionosphere, *Nature*, *157*, 691, doi:10.1038/157691a0.

Bailey, G. J., Y. Z. Su, and K.-I. Oyama (2000), Yearly variations in the low-latitude topside ionosphere, *Ann. Geophys.*, *18*, 789–798, doi:10.1007/s00585-000-0789-0.

Bankov, L., R. Heelis, M. Parrot, J.-J. Berthelier, P. Marinov, and A. Vassileva (2009), WN4 effect on longitudinal distribution of different ion species in the topside ionosphere at low latitudes by means of DEMETER, DMSP-F13 and DMSP-F15 data, *Ann. Geophys.*, *27*, 2893–2902, doi:10.5194/angeo-27-2893-2009.

Bilitza, D. (1975), Models for the relationship between electron density and temperature in the upper ionosphere, *J. Atmos. Terr. Phys.*, *37*, 1219–1222, doi:10.1016/0021-9169(75)90193-2.

Bilitza, D. (1987), Description of the mean behavior of ionospheric plasma temperature, *Adv. Space Res.*, *7*, 93–98, doi:10.1016/0273-1177(87)90280-8.

Bilitza, D., and W. R. Hoegy (1990), Solar activity variation of ionospheric plasma temperatures, *Adv. Space Res.*, *10*, 81–90, doi:10.1016/0273-1177(90)90190-B.

Brace, L. H., and R. F. Theis (1978), An empirical model of the interrelationship of electron temperature and density in the daytime thermosphere at solar minimum, *Geophys. Res. Lett.*, *5*, 275–278, doi:10.1029/GL005i004p00275.

England, S. L., S. Maus, T. J. Immel, and S. B. Mende (2006), Longitudinal variation of the E region electric fields caused by atmospheric tides, *Geophys. Res. Lett.*, *33*, L21105, doi:10.1029/2006GL027465.

England, S. L., T. J. Immel, and J. D. Huba (2008), Modeling the longitudinal variations in the postsunset far-ultraviolet OI airglow using the SAMI2 model, *J. Geophys. Res.*, *113*, A01309, doi:10.1029/2007JA012536.

Fang, T. W., A. D. Richmond, J. Y. Liu, A. Maute, C. H. Lin, C. H. Chen, and B. Harper (2008), Model simulation of the equatorial electrojet in the Peruvian and Philippine sectors, *J. Atmos. Sol. Terr. Phys.*, *70*, 2203–2211, doi:10.1016/j.jastp.2008.04.021.

Fejer, B. G. (1991), Low latitude electrodynamic plasma drifts: A review, *J. Atmos. Terr. Phys.*, *53*, 677–693, doi:10.1016/0021-9169(91)90121-M.

Forbes, J. M. (1981), The equatorial electrojet, *Rev. Geophys.*, *19*, 469–504, doi:10.1029/RG019i003p00469.

Forbes, J. M., X. Zhang, E. R. Talaat, and W. Ward (2003), Nonmigrating diurnal tides in the thermosphere, *J. Geophys. Res.*, *108*(A1), 1033, doi:10.1029/2002JA009262.

Forbes, J. M., X. Zhang, S. Palo, J. Russell, C. J. Mertens, and M. Mlynczak (2008), Tidal variability in the ionospheric dynamo region, *J. Geophys. Res.*, *113*, A02310, doi:10.1029/2007JA012737.

Forbes, J. M., S. L. Bruinsma, X. Zhang, and J. Oberheide (2009), Surface-exosphere coupling due to thermal tides, *Geophys. Res. Lett.*, *36*, L15812, doi:10.1029/2009GL038748.

Hagan, M. E., A. Maute, R. G. Roble, A. D. Richmond, T. J. Immel, and S. L. England (2007), Connections between deep tropical clouds and Earth's ionosphere, *Geophys. Res. Lett.*, *34*, L20109, doi:10.1029/2007GL030142.

Häusler, K., and H. Lühr (2009), Nonmigrating tidal signals in the upper thermospheric zonal wind at equatorial latitudes as observed by CHAMP, *Ann. Geophys.*, *27*, 2643–2652, doi:10.5194/angeo-27-2643-2009.

Hirao, K., and K.-I. Oyama (1970), An improved type of electron temperature probe, *J. Geomagn. Geoelectr.*, *22*, 393–402.

Immel, T. J., E. Sagawa, S. L. England, S. B. Henderson, M. E. Hagan, S. B. Mende, H. U. Frey, C. M. Swenson, and L. J. Paxton (2006), Control of equatorial ionospheric morphology by atmospheric tides, *Geophys. Res. Lett.*, *33*, L15108, doi:10.1029/2006GL026161.

Jin, H., Y. Miyoshi, H. Fujiwara, and H. Shinagawa (2008), Electrodynamics of the formation of ionospheric wave number 4 longitudinal structure, *J. Geophys. Res.*, *113*, A09307, doi:10.1029/2008JA013301.

Kakinami, Y., S. Watanabe, and K.-I. Oyama (2008), An empirical model of electron density in low latitude at 600 km obtained by Hinotori satellite, *Adv. Space Res.*, *41*, 1495–1499, doi:10.1016/j.asr.2007.09.031.

Kil, H., S.-J. Oh, M. C. Kelley, L. J. Paxton, S. L. England, E. Talaat, K.-W. Min, and S.-Y. Su (2007), Longitudinal structure of the vertical $\mathbf{E} \times \mathbf{B}$ drift and ion density seen from ROCSAT-1, *Geophys. Res. Lett.*, *34*, L14110, doi:10.1029/2007GL030018.

Kil, H., E. R. Talaat, S.-J. Oh, L. J. Paxton, S. L. England, and S.-J. Su (2008), Wave structures of the plasma density and vertical $\mathbf{E} \times \mathbf{B}$ drift in low-latitude F region, *J. Geophys. Res.*, *113*, A09312, doi:10.1029/2008JA013106.

Lebreton, J.-P., et al. (2006), The ISL Langmuir probe experiment processing onboard DEMETER: Scientific objectives, description and first results, *Planet. Space Sci.*, *54*, 472–486, doi:10.1016/j.pss.2005.10.017.

Lei, J., R. G. Roble, W. Wang, B. A. Emery, and S.-R. Zhang (2007), Electron temperature climatology at Millstone Hill and Arecibo, *J. Geophys. Res.*, *112*, A02302, doi:10.1029/2006JA012041.

Lin, C. H., A. D. Richmond, R. A. Heelis, G. J. Bailey, G. Lu, J. Y. Liu, H. C. Yeh, and S.-Y. Su (2005), Theoretical study of the low- and mid-latitude ionospheric electron density enhancement during the October 2003 superstorm: Relative importance of the neutral wind and the electric field, *J. Geophys. Res.*, *110*, A12312, doi:10.1029/2005JA011304.

Lin, C. H., W. Wang, M. E. Hagan, C. C. Hsiao, T. J. Immel, M. L. Hsu, J. Y. Liu, L. J. Paxton, T. W. Fang, and C. H. Liu (2007a), Plausible effect of atmospheric tides on the equatorial ionosphere observed by the FORMOSAT-3/COSMIC: Three-dimensional electron density structures, *Geophys. Res. Lett.*, *34*, L11112, doi:10.1029/2007GL029265.

Lin, C. H., C. C. Hsiao, J. Y. Liu, and C. H. Liu (2007b), Longitudinal structure of the equatorial ionosphere: Time evolution of the four-peaked EIA structure, *J. Geophys. Res.*, *112*, A12305, doi:10.1029/2007JA012455.

Lin, C. H., C. H. Chen, H. F. Tsai, C. H. Liu, J. Y. Liu, and Y. Kakinami (2011), Longitudinal structure of the mid- and low-latitude ionosphere observed by space-borne GPS receivers, in *Aeronomy of the Earth's*

Atmosphere and Ionosphere, IAGA Spec. Sopron Book Ser., vol. 2, edited by M. A. Abdu, D. Pancheva, and A. Bhattacharyya, chap. 27, pp. 363–374, Springer, New York, doi:10.1007/978-94-007-0326-1_27.

Liu, H., and S. Watanabe (2008), Seasonal variation of the longitudinal structure of the equatorial ionosphere: Does it reflect tidal influences from below?, *J. Geophys. Res.*, 113, A08315, doi:10.1029/2008JA013027.

Liu, H., C. Stolle, M. Förster, and S. Watanabe (2007), Solar activity dependence of the electron density in the equatorial anomaly regions observed by CHAMP, *J. Geophys. Res.*, 112, A11311, doi:10.1029/2007JA012616.

Liu, H., M. Yamamoto, and H. Lühr (2009), Wave-4 pattern of the equatorial mass density anomaly: A thermospheric signature of tropical deep convection, *Geophys. Res. Lett.*, 36, L18104, doi:10.1029/2009GL039865.

Namba, S., and K.-I. Maeda (1939), *Radio Wave Propagation*, 86 pp., Corona, Tokyo.

Oberheide, J., and J. M. Forbes (2008), Tidal propagation of deep tropical cloud signatures into the thermosphere from TIMED observations, *Geophys. Res. Lett.*, 35, L04816, doi:10.1029/2007GL032397.

Oya, H., T. Takahashi, and S. Watanabe (1986), Observation of low latitude ionosphere by the impedance probe on board the Hinotori satellite, *J. Geomagn. Geoelectr.*, 38, 111–123.

Oyama, K.-I., K. Schlegel, and S. Watanabe (1988), Temperature structure of plasma bubbles in the low latitude ionosphere around 600 km altitude, *Planet. Space Sci.*, 36, 553–567, doi:10.1016/0032-0633(88)90025-6.

Oyama, K.-I., S. Watanabe, Y. Su, T. Takahashi, and K. Hirao (1996), Season, local time, and longitude variations of electron temperature at the height of ~600 km in the low latitude region, *Adv. Space Res.*, 18, 269–278, doi:10.1016/0273-1177(95)00936-1.

Oyama, K.-I., D. R. Lakshmi, I. Kutiev, and M. A. Abdu (2005), Low latitude N_e and T_e variations at 600 km during 1 March 1982 storm from HINOTORI satellite, *Earth Planets Space*, 57, 871–878.

Pedatella, N. M., J. M. Forbes, and J. Oberheide (2008), Intra-annual variability of the low-latitude ionosphere due to nonmigrating tides, *Geophys. Res. Lett.*, 35, L18104, doi:10.1029/2008GL035332.

Ren, Z., W. Wan, L. Liu, B. Zhao, Y. Wei, X. Yue, and R. A. Heelis (2008), Longitudinal variations of electron temperature and total ion density in the sunset equatorial topside ionosphere, *Geophys. Res. Lett.*, 35, L05108, doi:10.1029/2007GL032998.

Sagawa, E., T. J. Immel, H. U. Frey, and S. B. Mende (2005), Longitudinal structure of the equatorial anomaly in the nighttime ionosphere observed by IMAGE/FUV, *J. Geophys. Res.*, 110, A11302, doi:10.1029/2004JA010848.

Scherliess, L., D. C. Thompson, and R. W. Schunk (2008), Longitudinal variability of low-latitude total electron content: Tidal influences, *J. Geophys. Res.*, 113, A01311, doi:10.1029/2007JA012480.

Schunk, R. W., and A. F. Nagy (1978), Electron temperatures in the *F* region of the ionosphere: Theory and observations, *Rev. Geophys.*, 16, 355–399, doi:10.1029/RG016i003p00355.

Su, Y. Z., G. J. Bailey, and K.-I. Oyama (1998), Annual and seasonal variations in the low-latitude topside ionosphere, *Ann. Geophys.*, 16, 974–985, doi:10.1007/s00585-998-0974-0.

Wan, W., L. Liu, X. Pi, M.-L. Zhang, B. Ning, J. Xiong, and F. Ding (2008), Wavenumber-4 patterns of the total electron content over the low latitude ionosphere, *Geophys. Res. Lett.*, 35, L12104, doi:10.1029/2008GL033755.

Watanabe, S., and K.-I. Oyama (1996), Effects of neutral wind on the electron temperature at a height of 600 km in the low latitude region, *Ann. Geophys.*, 14, 290–296, doi:10.1007/s00585-996-0290-5.

Watanabe, S., K.-I. Oyama, and M. A. Abdu (1995), Computer simulation of electron and ion densities and temperatures in the equatorial *F* region and comparison with Hinotori results, *J. Geophys. Res.*, 100, 14,581–14,590, doi:10.1029/95JA01356.

Y. Kakinami, Institute of Seismology and Volcanology, Hokkaido University, Kita 10 Nishi 8, Kita-ku, Sapporo 060-0810, Japan. (kaki@jupiter.ss.ncu.edu.tw)

M. Kamogawa, Department of Physics, Tokyo Gakugei University, 4-1-1 Nukuikitamachi, Koganeishi, Tokyo 184-0015, Japan.

C. H. Lin, Earth Dynamic System Research Center, National Cheng Kung University, No. 1, University Rd., Tainan 701, Taiwan.

J. Y. Liu, Institute of Space Science, National Central University, No. 300, Jhongda Rd., Jhongli 32001, Taiwan.

M. Parrot, Laboratoire de Physique et Chimie de l'Environnement et de l'Espace, 3A, Avenue de la Recherche Scientifique, 45071 Orléans CEDEX 2, France.

S. Watanabe, Department of Cosmoscience, Hokkaido University, Kita 10 Nishi 8, Kita-ku, Sapporo 060-0810, Japan.